Simulation Approach of the Asynchronous Machine Module for Students in the Laboratory

David Cárdenas Villacrés , Carlos Chavez , Otto Astudillo , Alexader Emanuel Torres *

Posted Date: 10 April 2026

doi: 10.20944/preprints202604.0773.v1

Keywords: asynchronous machine; torque; stator

 doi:10.20944/preprints202604.0773.v1

Article

Simulation Approach of the Asynchronous Machine Module for Students in the Laboratory

David Cárdenas Villacrés [1,†,‡], Carlos Chavez [2,‡,‡], Otto Astudillo [3,‡,‡] and Alexader Emanuel Torres [4,*,‡,‡]

[1] Telecommunication Engineering , Telecommunication Systems Research Group (GISTEL), Universidad Politécnica Salesiana, Campus Centenario, Chambers 227 y 5 de Junio Guayaquil, Ecuador
[2] Electrical Engineering , SMARTECH, Universidad Politécnica Salesiana, Campus Centenario, Chambers 227 y 5 de Junio Guayaquil, Ecuador
[3] Electrical Engineering , Universidad Politécnica Salesiana, Campus Centenario, Chambers 227 y 5 de Junio Guayaquil, Ecuador
[4] Electronic Engineering , SMARTECH, Universidad Politécnica Salesiana, Campus Centenario, Chambers 227 y 5 de Junio Guayaquil, Ecuador
* Correspondence: atorresr@ups.edu.ec
† Current address: GISTEL, Politecnica Salesiana University, Cuenca, Ecuador
‡ These authors contributed equally to this work.

Abstract

This paper presents the simulation of the Asynchronous Machine Module, making use of the LabView tool to make the graphical presentation of it, simulating its real behavior at the time of performing the practices, thus allowing the prediction of the state of the Variables of the induction motor according to its operation. With the data obtained from the simulation carried out in Simulink it was possible to observe the ideal behavior of the machine and the realization of the simulation in LabVIEW in order to later take data in a practical way and being able to compare by error percentage having low results.

Keywords: asynchronous machine; torque; stator

1. Introduction

Asynchronous machines, which are of constant use in industries due to their simplicity of construction and use, have been an indispensable cause of study and analysis of the variables that govern their behavior; therefore, future electrical engineers, this is an important part of knowledge [1,2]. With the present project it is possible to perform the simulation of the Asynchronous Machine Module performing different types of tests and thus analyzing the behavior of the same taking values such as current, speed and torque; in addition, the curves of the data taken from the different practices such as testing the machine under vacuum, by variation of the resistant torque, braking maneuver by injection of direct current will be plotted through the programming done in the Matlab and LabView® tool [3].

The use of LabVIEW® for programming enables an intuitive graphical development environment based on functional blocks rather than traditional code, simplifying the understanding of system behavior. This platform not only allows real-time acquisition of data from measurement instruments integrated into the Asynchronous Machine Module [4], but also provides a virtual interface that replicates the physical instrumentation. When combined with MATLAB-based simulations, which model the theoretical and dynamic behavior of the machine, LabVIEW® serves as a complementary tool that validates simulated responses through the acquisition of experimental data. This integration enhances the didactic process, allowing students to correlate the simulated scenarios with practical outcomes, thus reinforcing the theoretical concepts covered in class [5].

 doi:10.20944/preprints202604.0773.v1

2. Materials and Methods

The asynchronous or induction machine is defined as a rotating electrical machine in which there is no synchronism between the magnetic fields generated in the stator and the rotational speed of the rotor [6]. Its functioning or operation is based on the application of Faraday's law to a conductor [7], which states that voltage generation is possible when there is any change in the magnetic environment in which a conductor is located [3].

A fundamental aspect of the asynchronous machine that generally works or functions as a motor is that the three stator coils are 120 ° out of phase in space [8]. When electric current is injected into these windings, a rotating sine wave m.m.f. distributed sinusoidally around the periphery of the air gap produces a rotating flow of velocity [9].

Another aspect that must be considered is the design of the rotor, as this influences the starting torque that, being at rest, it has a state of inertia generating a resistant torque and increasing its current from 6 to 12 times its nominal value, since it needs to break its inertia [10–12].

The simulation with the LabVIEW® tool of the Asynchronous Machine Module requires first a data acquisition that will be performed through a simulation of the induction motor in Simulink of Matlab®. The tests performed were the vacuum test, torque resistance variation test, voltage variation starting test, and shunting test. voltage variation and braking maneuvering test by direct current injection. The data and results of these tests will be shown in the graphical interface previously created in LabView in order to perform the respective analysis of current, speed, and torque of each of the tests with respect to the practices performed in the module. The analysis of these tests will be performed using the error percentage, thus determining the reliability of the data [13].

2.0.1. Determination of Parameters

The main feature of an asynchronous machine, which generally works or functions as a motor, is that the stator winding consists of three windings offset by 120 ° in space [14]. When electrical current is injected from the frequency feeder Fr, a rotating wave of f.m.m. is produced, distributed sinusoidally around the periphery of the air gap, producing a rotating flux of velocity flux [15,16].

$$N_S = \frac{60 \cdot F_r}{p} \tag{1}$$

Equation 1 Rotational speed of the magnetic field.

Where:

NS = the synchronous speed of the rotating flow.
Fr = the frequency of the electrical current from the power supply.
P = the number of pairs of poles.

In the study of electrical machines, the following applies:

$$N_s > N_r \tag{2}$$

Equation 2 Field ratio

This inequality represents that the speed of the rotating magnetic field (N_s) is always higher than the mechanical speed of the rotor (N_r) in induction motors.

This is also referred to as slip and can be expressed as follows [6]:

Absolute slip:

$$S = N_s - N_r \tag{3}$$

Equation 3 Absolute slip of the induction motor

Relative slippage:

$$S\% = \left(\frac{N_s - N_r}{N_s}\right) \times 100\% \tag{4}$$

Equation 4 Relative slip of the induction motor

 doi:10.20944/preprints202604.0773.v1

The induced torque must be greater than the resistant torque for the motor to start, knowing that there are two induced torques, one due to the bars surrounding the rotor and the other due to the rotor itself.

$$T_{\text{ind}} > T_{\text{res}} \tag{5}$$

Equation 5 Torque induction

$$T_{\text{ind}} = n \cdot l \cdot B \cdot I \cdot r \tag{6}$$

Equation 6 Induced torque induction motor

Where:

It can be seen that the equivalent circuit of the motor is similar to that of the transformer, which produces a voltage in the secondary winding when voltage is supplied to the primary winding; while, when the motor stator is connected to a voltage source, the magnetic field generated in it produces a secondary magnetic field in the rotor. These magnetic fields interact with each other, causing the rotor to rotate, but with a difference between the speeds of these fields [12].

The stator circuit consists of a resistor and a coil leakage reactance. On the other hand, the stator circuit consists of a resistance and inductance of the same inductor, as well as a variable resistance defined by the mechanical load on the motor [6]. Another variable that must be considered is the frequency in the rotor, which is defined by the slip of the machine, so the rotor variables depend on this frequency.

It can be seen that the equivalent circuit Figure 1 of the motor is similar to that of the transformer, which produces a voltage in the secondary winding when voltage is supplied to the primary winding; while, when the motor stator is connected to a voltage source, the magnetic field generated in it produces a secondary magnetic field in the rotor. These magnetic fields interact with each other, causing the rotor to rotate, but with a difference between the speeds of these fields [17]. The stator circuit consists of a resistance and a coil leakage reactance. On the other hand, the stator circuit consists of a resistance and inductance from the same inductor, as well as a variable resistance defined by the mechanical load on the motor. Another variable that must be considered is the frequency in the rotor, which is defined by the slip of the machine, so the rotor variables depend on this frequency [18]. When there is current in the rotor circuit, there is also an electrical equation that is equivalent to the mechanical load of the motor and is defined as:

$$I_2 = \frac{E_2}{Z_2} \tag{7}$$

The rotor current is given by Equation 7:

Rotor Current Analysis

The rotor current in an induction motor is given by 8:

$$I_2 = \frac{sE_2}{z_2} \tag{8}$$

$$I_2 = \frac{sE_2}{R_2 + jSX_2} \tag{9}$$

Transformation of the Equation

It is divided by the displacement, leaving a single term:

$$I_2 = \frac{sE_2}{R_2 + jSX_2} \times \frac{1}{\frac{1}{s}} = \frac{E_2}{\frac{R_2}{s} + jX_2} \tag{10}$$

 doi:10.20944/preprints202604.0773.v1

$$I_2 = \frac{E_2}{\frac{R_2}{s} + jSX_2} \tag{11}$$

Resistance as a Function of Slip

With resistance depending on the slip of the machine:

$$I_2 = \frac{E_2}{R_2 + jSX_2 + R_2 - R_2} = \frac{E_2}{R_2 + jX_2 + \frac{R_2}{s} - R_2} \tag{12}$$

$$I_2 = \frac{E_2}{R_2 + jSX_2 + R_2 - R_2\left(\frac{1}{s} - 1\right)} \tag{13}$$

$$I_2 = \frac{E_2}{R_2 + jSX_2 + R_2\left(\frac{1}{s} - 1\right)} \tag{14}$$

Interpretation of Terms

- R_2 = Represents the resistance of the rotor
- $R_2\left(\frac{1}{s} - 1\right)$ = Represents the load resistance

Mechanical Load Resistance

The resistance of the mechanical load applied to the motor is given below.

$$R_C = R\left(\frac{1}{s} - 1\right) \tag{15}$$

The resistance to load is given by Equation 15.

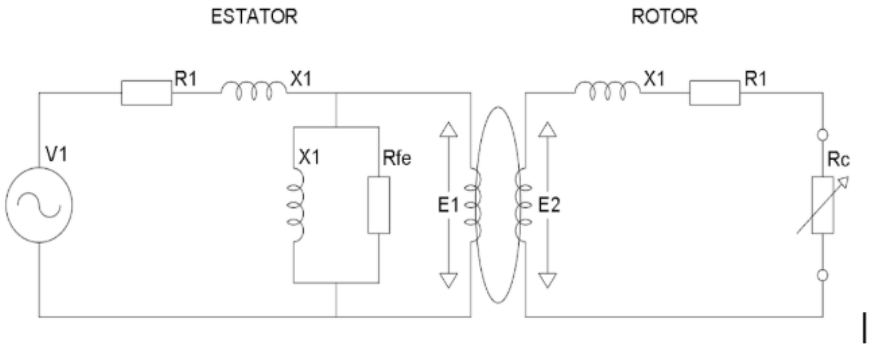

Figure 1. Equivalent diagram of the induction motor

2.0.2. Engine Plate Data

Table 1 presents the engine plate data of the asynchronous machine that we used in the test, with a speed of 1800 RPM, indicating that it is a 4 pole with a frequency of 60 Hz and allows us to connect the windings in star at 127 V or in delta at 220 V.

Table 1. Engine plate data

Power (P)	Voltage (V)	Frequency (f)	Speed ()	Rated Current (In)
3 HP	127 - 220 V	60 Hz	1800 r.p.m.	17,3 / 10 A

 doi:10.20944/preprints202604.0773.v1

Three-Phase Induction Motor Testing

Before performing the simulation, it was necessary to test the three-phase induction motor in order to determine the equivalent circuit diagram of the machine and thus configure the simulation parameters in Simulink. The tests were as follows:

Open circuit test (CA) This consists of running the asynchronous machine without a load resistive to the rotor shaft but with its nominal voltage values. After the test was performed, the data shown in the table was obtained. Table 2:

Table 2. Data obtained from the open circuit (AC) test

VPromedio	VFase	IPromedio
218 V	125,86 V	5,38 A

Locked rotor test (RB) This consists of applying a resistant torque to the rotor shaft, preventing it from moving when energized and reaching its rated current. After the test was performed, the data obtained can be seen in the table. Table 3:

Table 3. Data obtained from the blocked rotor test

VPromedio	VFase	IPromedio
54 V	31,18 V	9,88 A

Direct current (DC) voltage test This consists of supplying DC voltage to the motor coils, thereby obtaining voltage and current to determine the motor's resistance. After the experiment, the following data was obtained, which can be seen in the table below. Table 4:

Table 4. Data obtained from the DC voltage test

VDC	IDC
2,9 V	2,6 A

Determination of parameters

Using the values shown in the table, it is possible to calculate the open circuit impedance, thus obtaining the following:

$$|Z_{\text{ca fase}}| = \frac{V_{\text{fase}}}{I_{\text{fase}}} \tag{16}$$

$$|Z_{\text{ca fase}}| = \frac{125,86\,\text{V}}{5,38\,\text{A}} \tag{17}$$

$$|Z_{\text{ca fase}}| = 23,4\,\Omega \tag{18}$$

Using the values shown in the following table, it is possible to calculate the resistance of the stator of the asynchronous machine, thus obtaining the following:

$$R_1 = \frac{V_{\text{dc}}}{2 \times I_{\text{dc}}} \tag{19}$$

$$R_1 = \frac{2,9\,\text{V}}{2 \times 2,6\,\text{A}} = 0,56\,\Omega \tag{20}$$

Taking into account the equivalent circuit diagram Figure 2 the following values are obtained.

 doi:10.20944/preprints202604.0773.v1

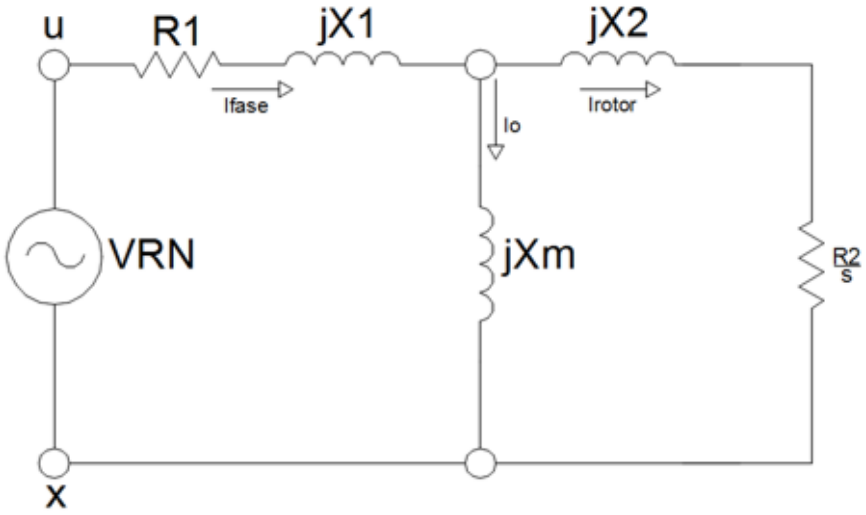

Figure 2. Equivalent circuit

Equivalent Circuit of the Asynchronous Machine

Parameter calculation

Power per phase:

$$P_{\text{fase}} = \frac{P_{\text{RB (3}\varnothing\text{)}}}{3} \tag{21}$$

$$P_{\text{fase}} = \frac{530\,\text{W}}{3} = 176,7\,\text{W} \tag{22}$$

Locked rotor impedance:

$$Z_{\text{RB}} = \frac{V_{\text{RB}}}{I_{\text{RB}}} \angle \left(\frac{P_{\text{f RB}}}{V_{\text{RB}} \times I_{\text{RB}}} \right) \tag{23}$$

$$Z_{\text{RB}} = \frac{31,18\,\text{V}}{9,88\,\text{A}} \angle \left(\frac{176,7\,\text{W}}{31,18\,\text{V} \times 9,88\,\text{A}} \right) = 3,16 \angle 54,9^{\circ}\,\Omega \tag{24}$$

Representation in rectangular coordinates is necessary to determine the resistance and reactance of the locked rotor, thus having the following:

$$Z_{\text{RB}} = (R_{\text{RB}} + jX_{\text{RB}}) \tag{25}$$

$$Z_{\text{RB}} = (1,81 + j2,58)\,\Omega \tag{26}$$

$$R_{\text{RB}} = 1,81\,\Omega \tag{27}$$

$$X_{\text{RB}} = j2,58\,\Omega \tag{28}$$

Rotor resistance (R_2):

$$R_{\text{RB}} = R_1 + R_2 \tag{29}$$

$$R_2 = R_{\text{RB}} - R_1 \tag{30}$$

$$R_2 = 1,81\,\Omega - 0,56\,\Omega = 1,25\,\Omega \tag{31}$$

Rotor and stator reactance (X_1 y X_2):

 doi:10.20944/preprints202604.0773.v1

$$X_{RB} = X_1 + X_2 \tag{32}$$

$$X_1 = X_2 = \frac{j2,58\,\Omega}{2} = j1,29\,\Omega \tag{33}$$

Magnetization inductance (X_M):

$$X_M = |Z_{\text{ca fase}}| - X_1 \tag{34}$$

$$X_M = j23,4\,\Omega - j1,29\,\Omega \tag{35}$$

$$X_M = j22,11\,\Omega \tag{36}$$

2.1. Simulation

2.1.1. Simulink

Before the simulation of the asynchronous machine module in the LabView® software, an ideal simulation of the asynchronous machine was performed on the Simulink platform of Matlab®, and these data obtained for current, speed, and torque for each practice proposed in this monograph will be imported to Excel to compare with the data obtained in a practical way and presented in LabView®. To make a comparison of the simulation of an ideal motor vs. the data obtained in the laboratory of machines I and II and then verify the percentage of error that exists between them. The results obtained from the different practices and the simulation will be used to perform an analysis of current, speed, torque in each test, to verify the behavior of the asynchronous machine, Figure 3.

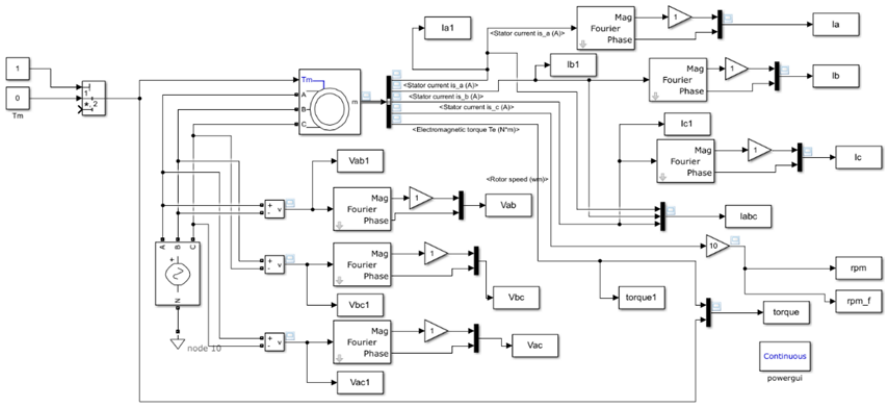

Figure 3. Simulation in Matlab Simulink

2.1.2. Labview

The tests performed in the simulation were:

- Vacuum testing of electrical machines
- Resistance torque variation test: This test was performed to determine the variation of different motor operating parameters by varying its operating conditions with a load of 1.2 Nm.

For space reasons, the graphic interface of the resistant torque with a load of 1.2 Nm. will be shown, for which we will display the main menu as shown in Figure 4.

 doi:10.20944/preprints202604.0773.v1

Figure 4. Test menu for torque resistance variation

3. Results

Before performing the analysis in a specific load case, the behavior of the machine is analyzed considering basic tests of the same, taking into account both Matlab and LabVIEW software for data acquisition. No-load test

In Figure 5, it can be seen that the motor consumes up to 50 A during startup and stabilizes 1.3 seconds after being energized; after that, its nonload consumption is approximately 5 A. Current vs. time

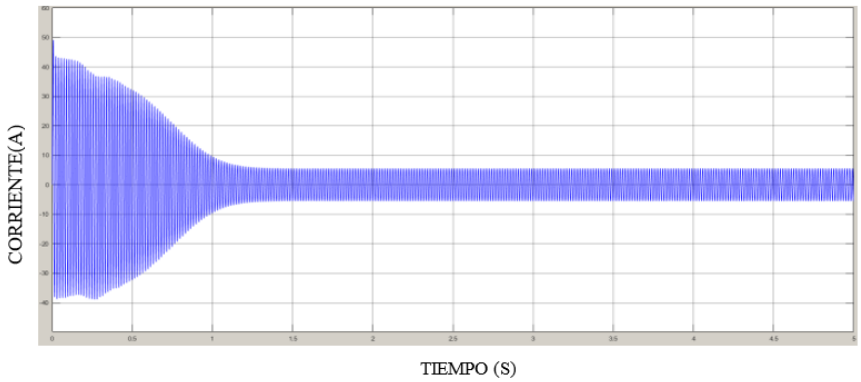

Figure 5. Vacio Corriente Tiempo Matlab

For Figure 6, the data acquired using LabVIEW confirm the behavior observed in Matlab: the starting current reaches high values during the first few moments, stabilizing at around 5 A once the

 doi:10.20944/preprints202604.0773.v1

motor overcomes its inertia and enters a steady state. The slight difference between the waveforms obtained in both environments can be attributed to the latency inherent in the acquisition system and to small fluctuations in the supply voltage, without compromising the validity of the results. This coincidence supports the reliability of the measurement, allowing us to conclude that the no-load consumption of the motor remains stable after the transient period.

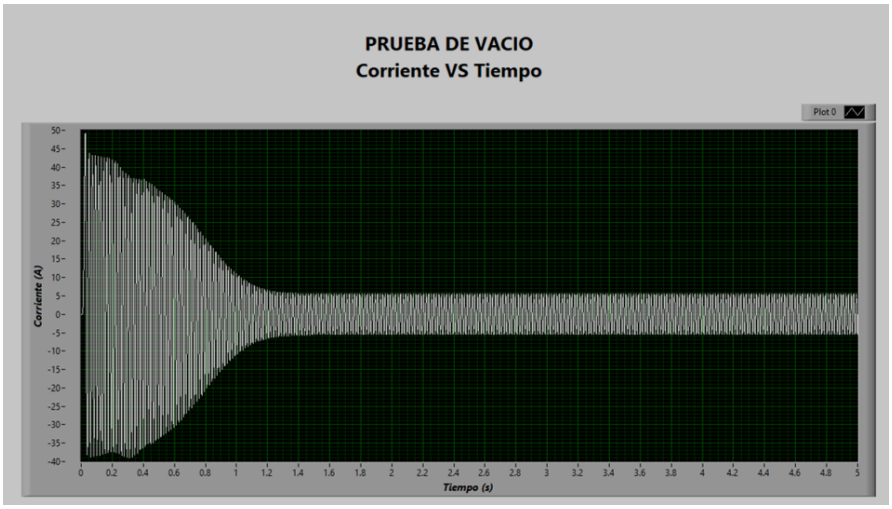

Figure 6. Vacio Corriente Tiempo Labview

In Figure 7, it can be seen that after overcoming its inertia, the motor begins to increase its speed exponentially until it stabilizes after 1.5 seconds at approximately 1800 rpm.

Speed vs. time

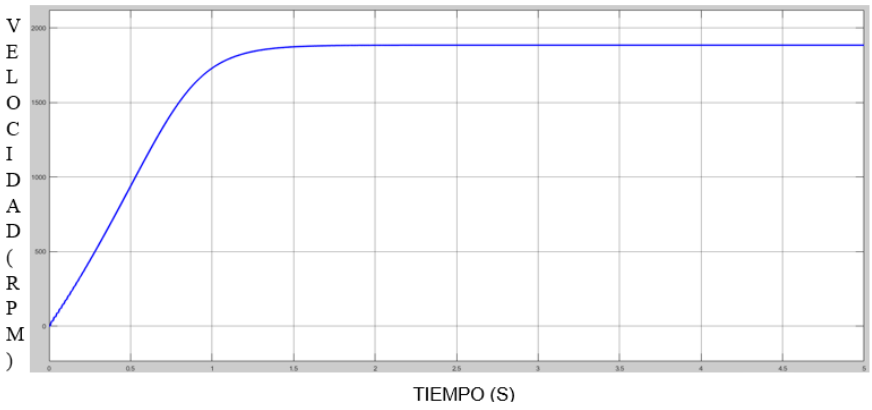

Figure 7. Vacio Velocidad Tiempo Matlab

In Figure 8, the speed record in LabVIEW faithfully reproduces the progressive acceleration of the motor: after exceeding the starting torque, the machine increases its speed almost exponentially, reaching approximately 1800 rpm in around 1.5 s. Minimal variations from the behavior simulated in Matlab may be due to the time resolution of the acquisition system or mechanical irregularities inherent to the shaft. However, the overall profile confirms that the model accurately reproduces the actual dynamics, ensuring the relevance of the parameters adopted for further analysis.

 doi:10.20944/preprints202604.0773.v1

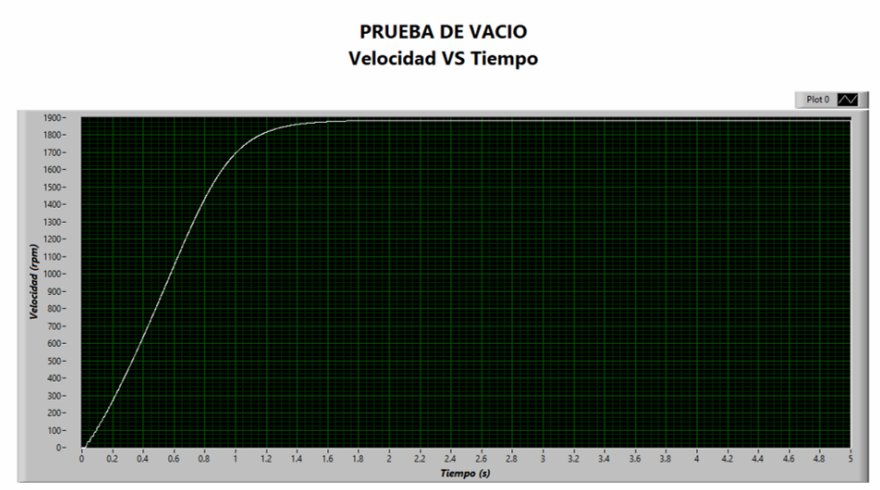

Figure 8. Vacio Velocidad Tiempo Labview

In Figure 9, it can be seen that the motor requires a torque of approximately 40 N.m to overcome its own inertia until it stabilizes after 1.6 seconds.

Torque vs. Time

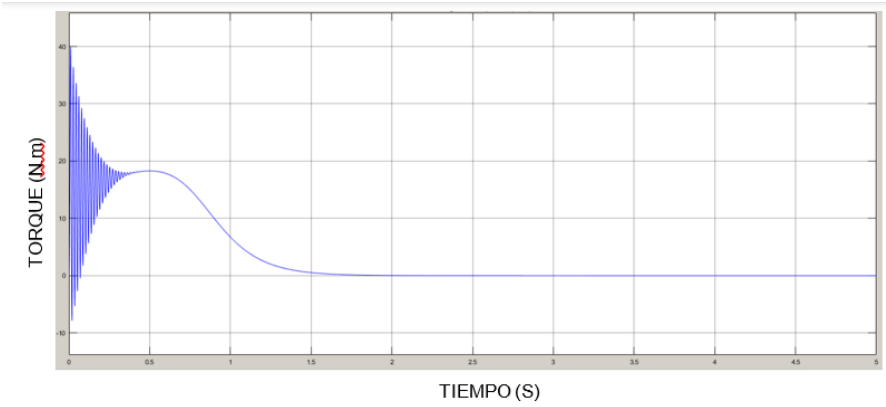

Figure 9. Vacio Torque Tiempo Matlab

In Figure 10, the data recorded with LabVIEW shows that the motor requires a torque of approximately 40 N·m during start-up, which is necessary to overcome its own inertia and friction losses in the bearings. After approximately 1.6 s, the torque tends to stabilize at a very low level, consistent with the no-load operation. This similarity to the Matlab results validates the robustness of the measurement system and confirms that the experimental conditions were adequate to characterize the dynamic behavior of the motor.

 doi:10.20944/preprints202604.0773.v1

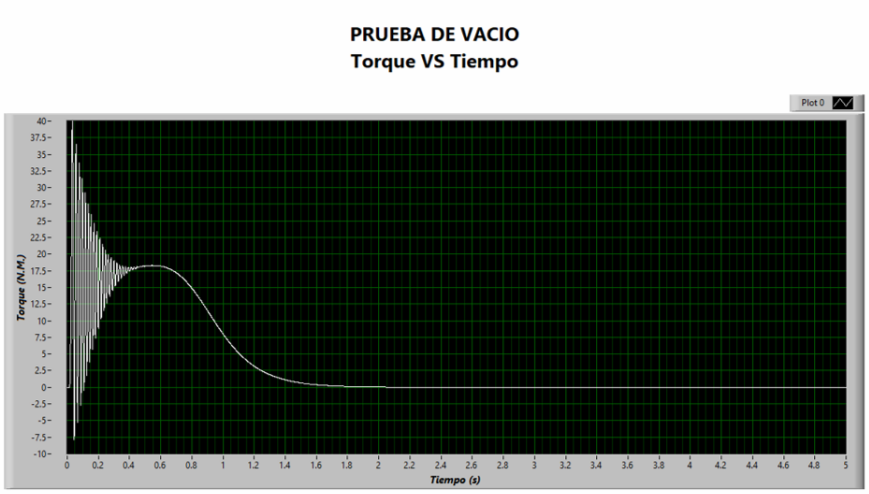

Figure 10. Vacio Torque Tiempo Labview

Likewise, the curve obtained in LabVIEW shows slight oscillations in torque during the first few moments, possibly associated with small irregularities in the power supply or microvibrations in the rotor-stator assembly. These variations do not affect the main conclusion: the theoretical model and experimental measurement describe the evolution of torque in transient and steady-state conditions with remarkable accuracy, providing a solid basis for continuing the analysis with specific load cases.

Figure 11 shows that most of the error points are in the range of 0 to 20 percent, but 13 of the 7,000 points taken are outside this range, so these simulated results are considered reliable. The 13 points that fall outside the 20 percent error range are part of the sample taken during engine start-up, so these errors may be caused by various factors, such as poor contact with the engine terminals at start-up, poor contact with a phase of the voltage regulator, or even rapid fluctuations in the supply voltage.

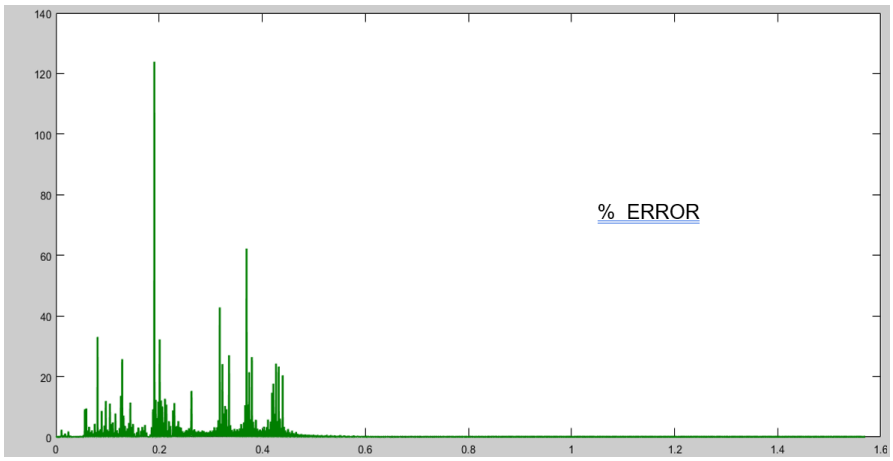

Figure 11. Análiss de Error

Considering the low error rate in the proposal, the analysis will continue with a specific functionality case.

Figure 12 illustrates the dynamic response of the induction motor during the star–delta starting sequence with 1.2 Nm. Figure 13 presents the time-domain current waveform, revealing a high inrush current at startup, which drops when the transition from the star to the delta connection occurs, showing the effectiveness of this strategy in reducing electrical stress. Finally, Figure 14 shows the development of the torque over time, indicating a stable behavior consistent with the observed current and speed variations.

 doi:10.20944/preprints202604.0773.v1

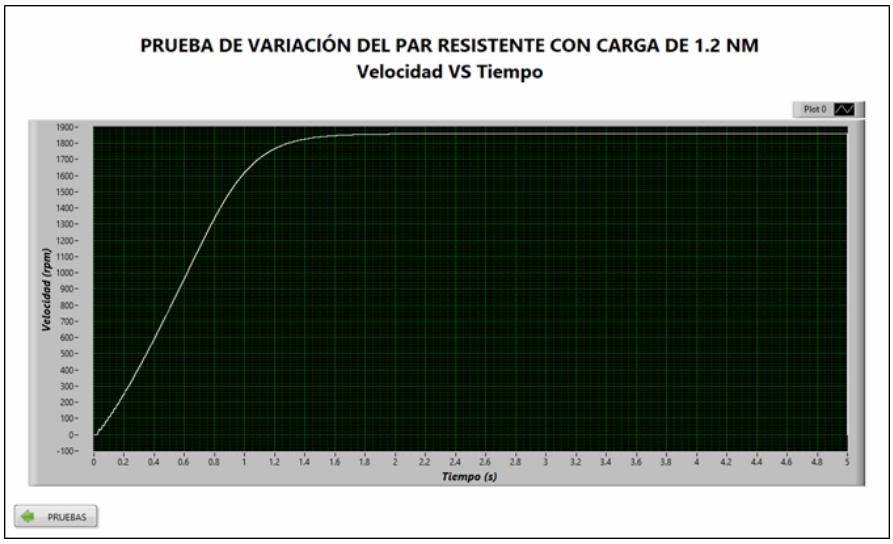

Figure 12. Rotor speed as a function of time during star–delta starting.

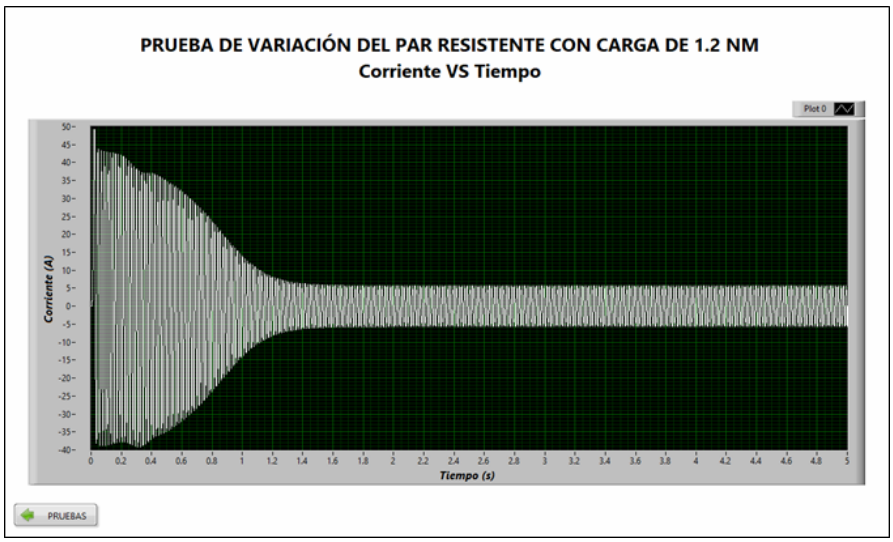

Figure 13. Time-domain current waveform during star–delta starting.

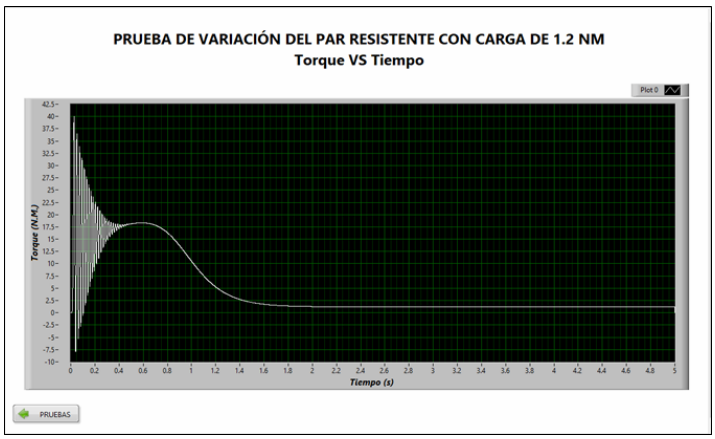

Figure 14. Torque evolution as a function of time during the start-up phase.

3.1. Current Analysis

In Figure 15 when comparing the simulated and plotted values in the programming (red curve) vs. the real measured values (blue curve) it is possible to determine the percentage error between them to verify if the simulation is reliable.

 doi:10.20944/preprints202604.0773.v1

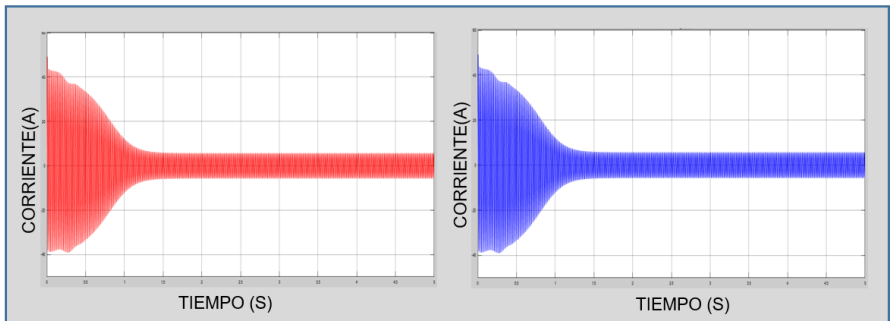

Figure 15. Comparison of current curves

In Figure 16 data can be observed that in the range of 1.5 seconds pass the 100 % error, this may be due to the fact that in that instant of time there was a change in the machine's own operating factors such as vibrations, loose terminals, cables in bad condition, motor malfunctions; however, these 87 points do not affect the analysis because it is a small part of the sample and the variation begins after the 6,500 data obtained.

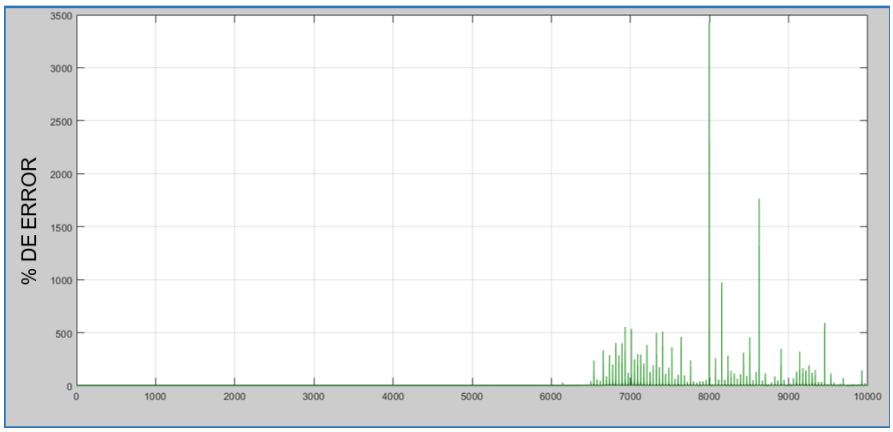

Figure 16. Error in % obtained in the comparison of currents

3.2. Speed Analysis

In Figure 17 Comparing the simulated and plotted values in the programming (red curve) vs. the real measured values (blue curve), it is possible to determine the percentage error between them to verify if the simulation is reliable.

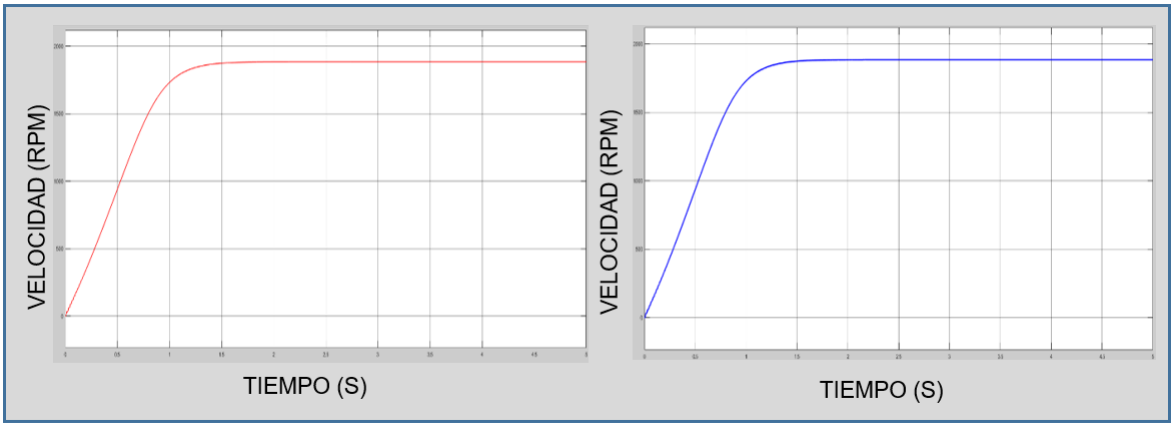

Figure 17. Comparison of speed curves

In Figure 18 it can be seen that the error percentage is minimal because it is between 0 and 0.2%, but after the first 2,000 points approximately the curve stabilizes, with this result it is shown that the simulation is reliable.

 doi:10.20944/preprints202604.0773.v1

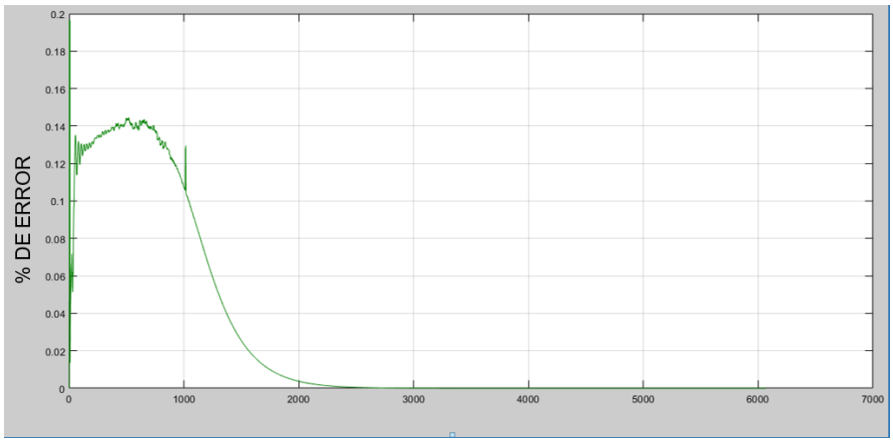

Figure 18. Error in % obtained in the speed comparison

The points between 0 and 2,000 are data taken during machine start-up, so these percentages may be higher than the rest due to bearing wear.

3.3. Torque Analysis

In Figure 19 comparing the simulated and plotted values in the programming (red curve) vs. the real measured values (blue curve), it is possible to determine the percentage error between them to verify if the simulation is reliable.

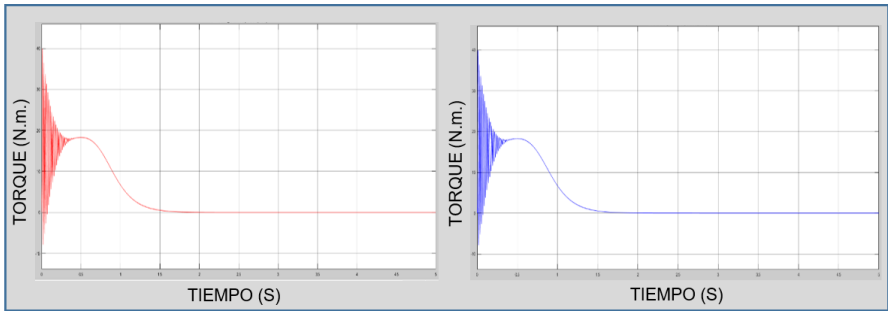

Figure 19. Comparison of torque curves

In Figure 20 it can be seen that the error percentage is low because the motor is without load, so the resistant torque will be zero and the motor must only overcome its own torque generated by the internal friction and the moment of inertia of the motor. The percentage of error is between 0 and 5%, thus confirming the reliability of the simulated system.

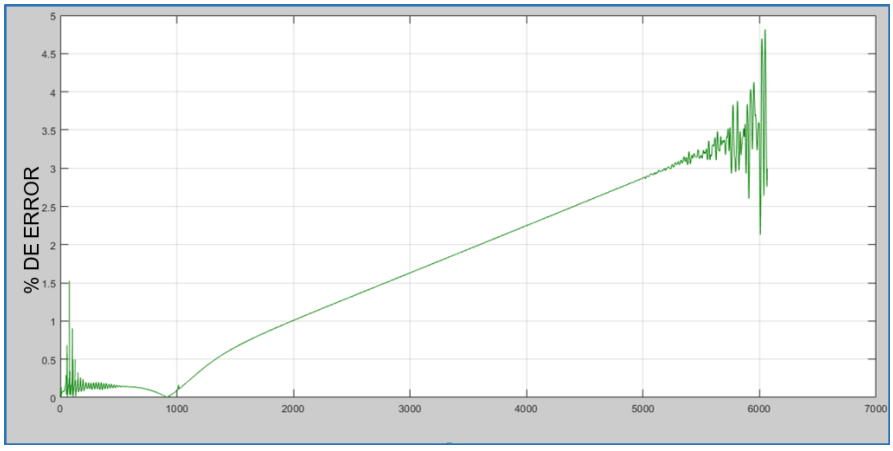

Figure 20. Error in % obtained in the torque comparison

 doi:10.20944/preprints202604.0773.v1

4. Discussion

The findings of this investigation demonstrate the viability and efficacy of the proposed simulation strategy to analyze asynchronous machines. The low error percentage obtained when comparing the data simulated in Simulink with actual laboratory measurements - below 5(%) for speed and torque and under 20(%) for current in most data points - confirms the accuracy of the implemented model. These error margins are particularly significant when considering the inherent variations in real-world motor operating conditions, where factors such as bearing wear, power supply fluctuations, and environmental conditions can introduce discrepancies. The consistency of the results validates the reliability of the simulation module for both educational purposes and technical analysis.

Detailed examination of error peaks during motor startup reveals crucial aspects of asynchronous machines' transient behavior. Although numerically scarce relative to the total sample size (only 13 out of 7000 points under no-load conditions and 87 in current analysis), the highest error points systematically coincide with initial operation moments where transient phenomena are most pronounced. This observation indicates that, while the simulated model effectively captures steady-state behavior, opportunities exist to enhance the representation of startup transients by incorporating more detailed models that account for variable friction and magnetic saturation effects.

The successful implementation of the graphical interface in LabVIEW® represents a significant advancement in the teaching methodology of electrical machinery. The capability of simultaneously visualizing theoretical (simulated) and practical (measured) behavior enables students to establish direct correlations between theoretical concepts and their manifestation in actual equipment. The general agreement between both curves, particularly evident in the speed analysis where the error remains between 0-0.2(%) after stabilization, strengthens the understanding of fundamental induction motor operation principles. This integrated approach not only optimizes practical work efficiency, but also promotes deeper and more meaningful learning by facilitating immediate experimental validation of theoretical concepts.

5. Conclusions

The simulation of the Asynchronous Machine Module was performed in the LabView® interface, graphically representing all its components, its uses, and procedures at the time of performing the practices established at the beginning of this work, which will facilitate the student to become familiar with the module at the time of performing a practice in person, since it allows him to identify the connections and the steps that must be executed, avoiding making mistakes that put at risk his well-being and that of his classmates. The programming was carried out in the LabView® software in which the main electrical parameters and characteristic curves of current, speed, and torque of the asynchronous machine can be observed in each of the established practices due to the data obtained prior to the development of the graphical interface of the Asynchronous Machine Module. Theoretical-practical applications were developed verifying the correct simulation by means of the analysis of the error percentage of each graph being this low in relation to the amount of data obtained, having as a result the verification of the efficiency of an ideal model and considering that some of these peaks within the error percentage were given to the internal and external factors that influence the performance of a motor such as environmental conditions, electrical faults, short between turns, short between phases; in addition, the own faults that are generated by the motor components in bearings, stator, and rotor. The comparative analysis between the results derived from the Matlab simulation and those obtained experimentally using LabVIEW showed a high degree of correspondence in the current, speed, and torque parameters. The discrepancies observed in the transient regime are mainly due to the temporal resolution limitations of the acquisition systems, as well as power supply fluctuations or mechanical factors intrinsic to the motor. These findings confirm the validity of the proposed model and the suitability of the methodological procedures applied, supporting the joint use of both environments as reliable tools for the dynamic characterization of electrical machines under no-load operating conditions. The error analysis showed that the outliers represent a marginal percentage of

 doi:10.20944/preprints202604.0773.v1

the total sample and are concentrated in the initial moments of start-up, when phenomena such as rotor inertia, internal friction, or instantaneous variations in supply voltage converge. The general consistency between the experimental data and the simulation results supports the robustness of the measurement system and the theoretical model used, providing a solid methodological basis for future research aimed at evaluating the performance of the machine under load conditions, optimizing start-up strategies, and refining control algorithms that promote energy efficiency and operational reliability.

Author Contributions: For research articles with several authors, a short paragraph specifying their individual contributions must be provided. The following statements should be used "Conceptualization, D.C.,C.C.,O.A. and A.T.; methodology, D.C.,C.C., O.Aand A.T.; software, D.C.,C.C., O.A and A.T.; validation, D.C.,C.C.,O.A and A.T.; formal analysis, D.C.,C.C.,O.A and A.T.; investigation, D.C.,C.C.,O.A and A.T.; resources, D.C.,C.C.,O.A and A.T.; data curation,D.C.,C.C.,O.A and A.T.; writing—original draft preparation, D.C.,C.C., O.A and A.T.; writing—review and editing, D.C.,C.C.,O.A and A.T.; visualization, D.C.,C.C.,O.A and A.T.; supervision, D.C.,C.C.,O.A and A.T.; project administration, D.C.,C.C.,O.A and A.T.; funding acquisition, D.C.,C.C., O.A and A.T. All authors have read and agreed to the published version of the manuscript.

Funding: Not applicable

Institutional Review Board Statement: Not applicable

Informed Consent Statement: Not applicable

Data Availability Statement: Not applicable

Acknowledgments: Not applicable

Conflicts of Interest: The authors declare that they have no known competing financial interest or personal relationships that could have appeared to influence the work reported in the manuscript.

References

1. Misra, H.; Gundavarapu, A.; Jain, A.K. Control Scheme for DC Voltage Regulation of Stand-Alone DFIG-DC System. *IEEE Transactions On Industrial Electronics* **2017**, *64*, 2700–2708. https://doi.org/10.1109/TIE.2016.2632066.
2. Lakhimsetty, S.; Surulivel, N.; Somasekhar, V.T. Improvised SVPWM Strategies for an Enhanced Performance for a Four-Level Open-End Winding Induction Motor Drive. *IEEE Transactions On Industrial Electronics* **2017**, *64*, 2750–2759. https://doi.org/10.1109/TIE.2016.2632059.
3. Hamla, H.; Rahmani, L.; Belhaouchet, N. A modified direct torque control with minimum torque ripple and constant switching frequency for induction motor drives. *International Transactions On Electrical Energy Systems* **2019**, *29*. https://doi.org/10.1002/2050-7038.12120.
4. Luo, Y.; Liu, C. A Simplified Model Predictive Control for a Dual Three-Phase PMSM With Reduced Harmonic Currents. *IEEE Transactions On Industrial Electronics* **2018**, *65*, 9079–9089. https://doi.org/10.1109/TIE.2018.2814013.
5. Hannan, M.A.; Abd Ali, J.; Ker, P.J.; Mohamed, A.; Lipu, M.S.H.; Hussain, A. Switching Techniques and Intelligent Controllers for Induction Motor Drive: Issues and Recommendations. *IEEE Access* **2018**, *6*, 47489–47510. https://doi.org/10.1109/ACCESS.2018.2867214.
6. Hara, T.; Aoyagi, S.; Ajima, T.; Iwaji, Y.; Takahata, R.; Sugiyama, Y. Neutral Point Voltage Model of Stator Windings of Permanent Magnet Synchronous Motors with Magnetic Asymmetry. In Proceedings of the 2018 XIII International Conference On Electrical Machines (ICEM). Int Conf Elect Machines Assoc; IEEE Ind Applicat Soc; IEEE Ind Elect Soc; Democritus Univ Thrace, Dept Elect & Comp Engn; Minist Environm & Energy, 2018, pp. 1611–1616. 13th International Conference on Electrical Machines (ICEM), Alexandroupoli, GREECE, SEP 03-06, 2018.
7. Qiu, H.; Zhang, Y.; Yang, C.; Yi, R. Influence of inverter voltage harmonics on the torque ripple of surface permanent magnet synchronous motor. *International Journal Of Applied Electromagnetics And Mechanics* **2020**, *62*, 403–414. https://doi.org/10.3233/JAE-190010.
8. Yoo, J.; Lee, J.; Sul, S.K.; Baloch, N.A. Stator Resistance Estimation Using DC Injection With Reduced Torque Ripple in Induction Motor Sensorless Drives. *IEEE Transactions On Industry Applications* **2020**, *56*, 3744–3754.

 doi:10.20944/preprints202604.0773.v1

11th Annual IEEE Energy Conversion Congress and Exposition (ECCE), Baltimore, MD, SEP 29-OCT 03, 2019, https://doi.org/10.1109/TIA.2020.2984189.

9. Liang, Z.; Hu, S.; Li, Z.; Tahir, M. Research on Master-Slave Windings Motor Drive System and Control Strategy. *IEEE Transactions On Industrial Electronics* **2023**, *70*, 88–98. https://doi.org/10.1109/TIE.2022.3156171.
10. Aihsan, M.Z.; Jidin, A.; Azizan, M.M.; Fahmi, M.I.; Hasikin, K. Flexible Sector Detector-Based Mismatch Supply Voltage in Direct Torque Control Doubly Fed Induction Machine: An Experimental Validation. *Alexandria Engineering Journal* **2023**, *74*, 689–704. https://doi.org/10.1016/j.aej.2023.05.060.
11. Guedida, S.; Tabbache, B.; Nounou, K.; Benbouzid, M. Direct Torque Control Scheme For Less Harmonic Currents And Torque Ripples For Dual Star Induction Motor. *Revue Roumaine Des Sciences Techniques-Serie Electrotechnique Et Energetique* **2023**, *68*, 331–338. https://doi.org/10.59277/RRST-EE.2023.68.4.2.
12. Tatte, Y.N.; Aware, M.V. Torque Ripple and Harmonic Current Reduction in a Three-Level Inverter-Fed Direct-Torque-Controlled Five-Phase Induction Motor. *IEEE Transactions On Industrial Electronics* **2017**, *64*, 5265–5275. https://doi.org/10.1109/TIE.2017.2677346.
13. Bodson, M. Speed Control for Doubly Fed Induction Motors With and Without Current Feedback. *IEEE Transactions On Control Systems Technology* **2020**, *28*, 898–907. https://doi.org/10.1109/TCST.2019.2898372.
14. Eldeeb, H.; Hackl, C.M.; Horlbeck, L.; Kullick, J. A unified theory for optimal feedforward torque control of anisotropic synchronous machines. *International Journal Of Control* **2018**, *91*, 2273–2302. https://doi.org/10.1080/00207179.2017.1338359.
15. Xiao, M.; Shi, T.; Yan, Y.; Xu, W.; Xia, C. Predictive Torque Control of Permanent Magnet Synchronous Motors Using Flux Vector. *IEEE Transactions On Industry Applications* **2018**, *54*, 4437–4446. 20th IEEE International Conference on Electrical Machines and Systems (ICEMS), Sydney, AUSTRALIA, AUG 11-17, 2017, https://doi.org/10.1109/TIA.2018.2833817.
16. Yang, S.; Ding, D.; Li, X.; Xie, Z.; Zhang, X.; Chang, L. A Novel Online Parameter Estimation Method for Indirect Field Oriented Induction Motor Drives. *IEEE Transactions On Energy Conversion* **2017**, *32*, 1562–1573. https://doi.org/10.1109/TEC.2017.2699681.
17. Bin, Z.; Lili, M.; Hao, D. Principle of Optimal Voltage Regulation and Energy-Saving for Induction Motor With Unknown Constant-Torque Working Condition. *IEEE Access* **2020**, *8*, 187307–187316. https://doi.org/10.1109/ACCESS.2020.3030936.
18. Lee, K.; Choi, H.g.; Ha, J.I. Power Capability Improvement of Interior Permanent Magnet Synchronous Motor Drives Using Capacitive Network. *IEEE Transactions On Industrial Electronics* **2020**, *67*, 10109–10120. https://doi.org/10.1109/TIE.2019.2962410.